



Currents and topography drive assemblage distribution on an active hydrothermal edifice

Fanny Girard^{a,*}, Jozée Sarrazin^a, Aurélien Arnaubec^b, Mathilde Cannat^c, Pierre-Marie Sarradin^a, Benjamin Wheeler^c, Marjolaine Matabos^a

^a Ifremer, EEP, F-29280 Plouzané, France

^b Ifremer, SM, F-83507 La Seyne Sur Mer, France

^c Marine Geoscience Group, Institut de Physique du Globe de Paris, CNRS, UMR 7154, Université Paris Diderot, Sorbonne Paris Cité, Paris cedex 05, France

ARTICLE INFO

Keywords:

Mid-Atlantic Ridge
Eiffel Tower
EMSO-Azores
Ecology
Imagery
3D photogrammetry
Deep-sea observatories
Topographic effects

ABSTRACT

The deep sea is characterized by a wide range of landscapes, including complex features where topography and currents interact to form highly heterogeneous habitats. In addition to a complex topography, hydrothermal vent environments are characterized by strong environmental gradients that structure the spatial distribution of biological communities. The role of vent fluid temperature and chemical composition on species distribution is now well understood, but investigations on the effects of the complex sulfide edifice topography are scarce. Here, we used a novel approach combining 3D photogrammetric reconstruction, *in situ* environmental measurements and modeling to characterize assemblage distribution on the active edifice Eiffel Tower (Lucky Strike, Mid-Atlantic Ridge). Through the analysis of a high-resolution 3D model of the edifice, we show that assemblage distribution along with hydrothermal activity vary with their position on the edifice. Although physical terrain variables had a minor effect on assemblage distribution, the distance from fluid exits explained the distribution of most assemblages. However, these particular variables did not significantly explain the distribution of medium-sized *Bathymodiolus azoricus* mussels, the dominant assemblage on the edifice. Similarly, proximity to fluid exits only partially accounted for the distribution of microbial mats throughout the edifice. By modeling the current-driven dispersion of hydrothermal plumes around the edifice, we demonstrated that differences in mussel sizes may be due to differences in exposure time to currents bringing plume material. For the first time, we provide evidence that hydrothermal plumes can affect faunal assemblages meters away from fluid exits and that this relatively long-distance effect of vent plumes can fully account for microbial mat distribution throughout the edifice. Our findings extend the area of influence of hydrothermal plumes on vent communities considerably beyond previous estimations and suggest that the interactions between bottom currents, topography and smoker locations should be further investigated and considered as important structuring factors at vents. This novel approach, allowing to cover large areas of the seafloor, is particularly well suited for deep environments where topography and currents interact to form complex oceanographic patterns (e.g. canyons, seamounts). Its application to larger areas and various ecosystems can significantly enhance our understanding of benthic communities' distribution at large.

1. Introduction

Understanding the environmental factors that explain species distribution is fundamental in conservation biology. Characterizing the link between environmental factors and species distribution at scales of kilometers is necessary to determine the location of marine protected areas (MPA) and establish MPA networks, but information on factors affecting the microdistribution (at scales of centimeters to meters) is just as important when assessing potential anthropogenic impacts. The

growing interest in deep-sea mining compels the need for knowledge on the factors influencing species distribution in the deep sea. Seafloor massive sulfide deposits on hydrothermal vents are among the most recent mining industry targets, and their extraction is expected to result in biodiversity loss through both direct and indirect impacts (Van Dover, 2014; Levin et al., 2016b; Van Dover et al., 2017). However, mining activities in the deep sea have not yet started, leaving a unique opportunity to develop regulatory frameworks for the conservation of vent ecosystems before extraction begins. Thus, collecting baseline

* Corresponding author.

E-mail address: fanny.girard13@gmail.com (F. Girard).

<https://doi.org/10.1016/j.pocean.2020.102397>

Received 23 May 2019; Received in revised form 22 June 2020; Accepted 26 June 2020

Available online 06 July 2020

0079-6611/ © 2020 The Authors. Published by Elsevier Ltd. This is an open access article under the CC BY-NC-ND license

(<http://creativecommons.org/licenses/by-nc-nd/4.0/>).

ecological data is now essential.

Hydrothermal vents are found in all oceans in areas where ocean crust is being created, such as mid-ocean ridges and back-arc basins (Fisher et al., 2007). Unlike most of the deep sea, vent ecosystems host extremely high faunal biomass (Grassle, 1985). Vent communities rely on chemoautotrophic microorganisms that can harness energy coming from the oxidation of reduced chemicals dissolved in the hot hydrothermal fluid. These microorganisms, either free-living or in symbiosis with metazoan species, form the basis of the food chain (Childress and Fisher, 1992). Although hydrothermal fluids can reach temperatures of ~400 °C (Spiess et al., 1980; Koschinsky et al., 2008), turbulent mixing with surrounding cold seawater leads to steep thermal and chemical gradients over short distances from the vents (Johnson et al., 1988; Le Bris et al., 2006). As a result, community spatial distribution is structured by fluid chemical composition and temperature, depending on the nutritional needs and temperature tolerance of organisms (Hessler, 1985; Tunnicliffe, 1991; Shank et al., 1998; Luther et al., 2001; Ravaux et al., 2013).

Spatial zonation relative to fluid exposure has been characterized for most known vent sites (East Pacific Rise (Hessler, 1985; Shank et al., 1998), Juan de Fuca Ridge (Sarrazin et al., 1997; Sarrazin et al., 1999), Mid-Atlantic Ridge (Copley et al., 2007; Cuvelier et al., 2009), Indian Ridge (Van Dover et al., 2001; Zhou et al., 2018), East Scotia Ridge (Marsh et al., 2012), western Pacific back-arc basins (Podowski et al., 2010; Tokeshi, 2011; Sen et al., 2013)). In these studies, faunal distribution was characterized using imaging techniques, such as video transects or photo mosaics of still images. Image analysis has the advantage of being non-destructive and allows the investigation of larger surfaces than physical sampling, making it an essential tool for studying community distribution and monitoring (Cuvelier et al., 2012). Although studies based on 2D image analysis have significantly contributed to our current knowledge on hydrothermal vent ecosystems, they did not consider the effects of the structural complexity of vent habitats on faunal distributions. As a result, perspective errors, likely to occur in rough terrains (Pizarro et al., 2009), may have affected the accuracy of some results (e.g. estimated surfaces or distances).

In addition, habitat complexity (generally measured as substratum roughness) can play a significant role in structuring benthic communities. In shallow marine environments, complex habitats are often associated with higher diversity or abundance of organisms than less complex ones (Heck and Wetstone, 1977; Eriksson et al., 2006, Koivisto and Westerbomb, 2010; Freestone and Osman, 2011). Moreover, habitat complexity can influence recruitment (Eckman, 1987; Petraitis, 1990; Köhler et al., 1999) and predation (Menge et al., 1985; Frandsen and Dolmer, 2002) by increasing the surface available for settlement, altering boundary layer flows, or providing shelter. Although not as well characterized, similar trends have been observed in non-reducing deep-sea environments (Buhl-Mortensen et al., 2010; McClain and Barry, 2010). However, while some studies have shown an effect of substratum type and complexity on benthic communities at hydrothermal vents (Kelly and Metaxas, 2008; Podowski et al., 2010; Goffredi et al., 2017), the only study that has investigated vent megafaunal distribution using 3D imaging found that terrain variables only played a minor role in structuring these communities (Gerdes et al., 2019).

In addition to its direct effects, habitat complexity can indirectly affect benthic faunal distribution by altering current flow. While surface-generated mesoscale eddies (Kontar and Sokov, 1994; Zhang et al., 2014; Aleynik et al., 2017) and hurricanes (Morozov and Velarde, 2008) can significantly increase current velocity above flat regions of the seafloor such as abyssal plains, low topography areas are generally associated with low mixing rates (Toole et al. 1994). On the opposite, rough topography can significantly enhance turbulent mixing as strong flows pass through narrow channels (Polzin et al., 1996, St Laurent and Thurnherr, 2007, Tippenhauer et al., 2015) and modify overall current hydrodynamics (Denny, 1988, Cannon et al., 1991, White et al., 2008).

As a result, depending on the scale considered, the interaction

between currents and topography or substratum complexity can influence larval dispersal, recruitment and food supply in the benthos (Walton, 1946, Mullineaux and Butman, 1990, Davies et al., 2009, Vic et al., 2018). At vents, current direction and velocity can also affect the dispersion of hydrothermal fluids, and thus their chemical composition and temperature, potentially affecting benthic communities (Little et al., 1988; Barreyre et al., 2014; Lee et al., 2015). For instance, studies have detected that tidal cycles, which modulate bottom currents (Tivey et al., 2002), affect the behavior of both chemosymbiotic and non-symbiotic fauna (Cuvelier et al., 2014, Lelièvre et al., 2017). One of these studies also linked variations in faunal abundance to surface storm-induced changes in currents (Lelièvre et al., 2017). Despite their potential influence on faunal distribution at hydrothermal vents, the interactions between topography, bottom currents and fluid exit locations have never been examined.

In this study, we investigated assemblage distribution on the active Eiffel Tower edifice (Lucky Strike vent field, Mid-Atlantic Ridge) through the analysis of a high-resolution 3D model of the entire edifice reconstructed using structure-from-motion photogrammetry (Westoby et al., 2012, Kwasnitschka et al., 2013). Eiffel Tower has been the subject of a large number of ecological studies since its discovery in the 1990s (Desbruyères et al., 2001, Cuvelier et al., 2009, De Busserolles et al., 2009, Cuvelier et al., 2011a, Cuvelier et al., 2011b, Sarrazin et al., 2015, Husson et al., 2017). It is dominated by *Bathymodiulus azoricus* (Cosel et al., 1999) mussel assemblages that segregate by size along fluid flow intensity and thermal gradients (Cuvelier et al., 2009). Although the distance from fluid exits and temperature explain the general spatial distribution of shrimp and mussel assemblages, micro-distribution patterns have remained partly unresolved. In particular, the distribution of medium-sized mussels – the prevailing mussel assemblage on Eiffel Tower – cannot be explained by temperature due to the mussels' wide thermal niche (Husson et al., 2017). Because bathymodiolin mussels are ubiquitous and represent one of the most common foundation species in chemosynthetic environments (Govenar, 2010), elucidating drivers of their distribution is of major importance. Furthermore, most vent sites (including Eiffel Tower) still lack information on factors driving the spatial distribution of other important members of hydrothermal ecosystems, such as microbial mats or peripheral fauna.

Here, we combined the analyses of the high-resolution 3D reconstruction of Eiffel Tower and environmental data (bottom currents and temperature) collected as part of the EMSO-Azores multidisciplinary observatory (<http://www.emso-fr.org/EMSO-Azores>) to (1) characterize the spatial distribution of benthic assemblages on Eiffel Tower, (2) test the effects of distance from hydrothermal venting features and terrain variables (roughness and slope) on faunal micro-distribution, and (3) model the effect of bottom currents, in interaction with edifice topography and smoker locations, on microbial mat and faunal distributions. Overall, we used a novel multidisciplinary approach to deepen our understanding of community distribution on an active vent edifice.

2. Materials and methods

2.1. Study site and data acquisition

The Lucky Strike (LS) hydrothermal vent field is located off the Azores at a depth of 1700 m, at the summit of a volcano in the axial valley of the Mid-Atlantic Ridge. This vent field extends over more than 1 km² and is one of the largest on the Mid-Atlantic Ridge (Langmuir et al., 1997). LS consists of about 20 active and inactive sites surrounding a central fossil lava lake (Fouquet et al., 1995). Eiffel Tower, located south-east of this lava lake, is one of the most active vent sites. It can be divided into two areas: the main structure, an 11 m high and 5 m wide sulfide tower, and a hydrothermally active “periphery” that extends about 10 m to the northwest of the tower (Fig. 1).

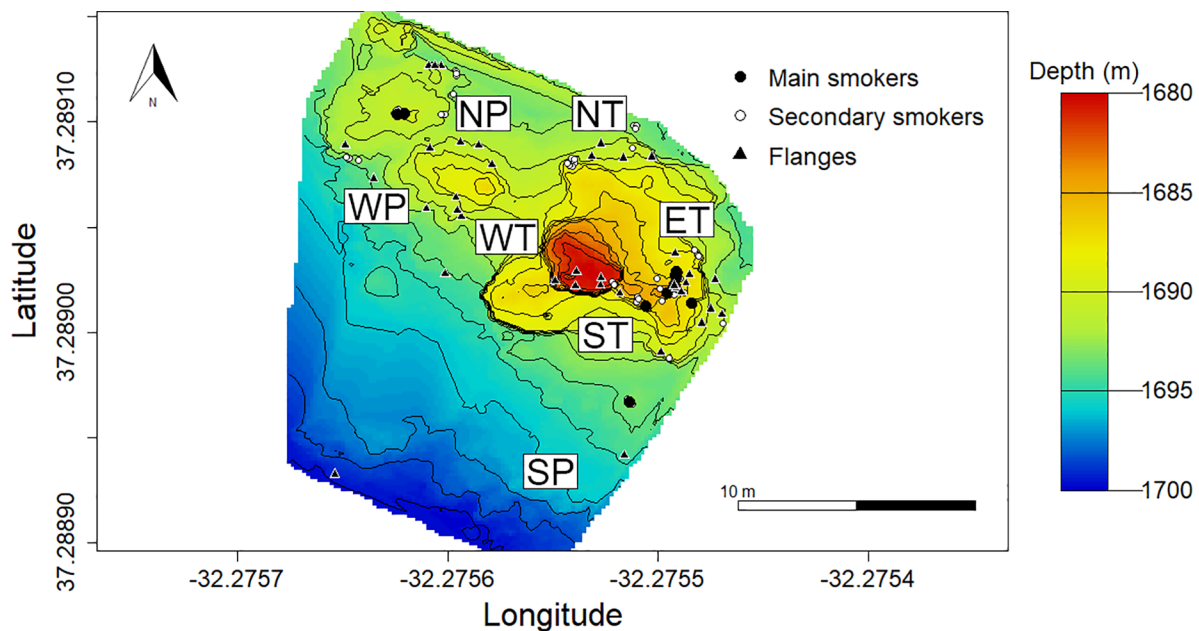


Fig. 1. Bathymetric map of Eiffel Tower showing the location of hydrothermal venting features (main and secondary smokers and flanges). The seven studied faces of the edifice are also labeled on the map. Tower: South (ST), West (WT), North (NT) and East (ET). Periphery: South (SP), West (WP), North (NP).

Video transects covering all faces of the edifice were carried out in 2015 using the remotely operated vehicle (ROV) *Victor6000* during the annual EMSO-Azores observatory maintenance expedition (Sarradin and Cannat, 2015). Lighting and camera zoom (minimum zoom) were kept constant throughout video acquisition, and the overlap between transects was maximized (> 50%). In addition, every effort was made to maintain a constant distance of ~1 m between the edifice and the ROV.

Video transects were then used for the 3D reconstruction of the entire edifice. Frame grabs were extracted from the video at a rate of 1 image every 3 s and imported into Matisse 3D (Ifremer software; Arnaubec et al. (2015)). A georeferenced 3D model of the entire edifice was then built using the “structure from motion” technique (Moulon et al. 2013; Supplementary Video S1). The reconstruction was scaled using the vehicle navigation system, which was based on the merging of data from an acoustic ultra-short baseline system (USBL), a doppler velocity log (Dvl) and fiber optic inertial units (Phins).

2.2. Fauna and substrata digitization

Fauna and substrata were digitized on the 3D model using 3DMetrics (Ifremer software under development). All substrata and faunal assemblages were digitized as polygons. Although assemblages could generally be identified on the 3D reconstruction, video transects were examined to confirm all identifications. Most assemblage/substratum categories were defined based on Cuvelier et al. (2009): dense beds of large *Bathymodiolus azoricus* mussels (assemblage 1), clumps of medium-sized mussels (assemblage 2), dispersed small mussels (assemblage 4), shrimp assemblages dominated by *Mirocaris fortunata* (Martin and Christiansen (1995); assemblage 3), bare substratum (sub1), and substratum with anhydrite precipitation (sub2). Mussel assemblages and bare substrata were divided into two sub-categories based on the absence (a) or presence (b) of a microbial cover (Fig. 2). In addition, assemblages and substrata that had not been quantified in previous studies, such as sulfide deposits, empty *B. azoricus* shell aggregates and non-vent endemic fauna (unidentified species of hydroids and zoanths), were digitized (Fig. 2). Once the entire edifice was digitized, surfaces covered by all assemblages and substrata, as well as the total surface of the edifice and of each face, were computed and percent covers estimated for all categories. For simplification,

substratum sub1a was not digitized and its surface was calculated on any given face by subtracting the surface covered by all the other assemblages/substrata from the face’s total surface.

Individual crabs of the species *Segonzacia mesatlantica* (Williams 1988), the most abundant solitary taxon on Eiffel Tower, were digitized as point layers (Fig. 2). For every crab identified on the edifice, the type of assemblage or substratum on which it was observed was recorded.

Both active smokers and flanges were also identified and digitized as point layers. Smokers were divided into two categories: “Main” smokers, characterized by a black plume rising several meters above the chimney and exhibiting high flow rates, and “secondary” smokers with focused but localized emissions of translucent fluid. As it was not always possible to determine whether a flange was active or not based on video transects, no distinction was made between active and inactive flanges. Similarly, it was generally not possible to identify diffuse venting emissions from the video sequences. Therefore, diffusion zones were not digitized. The locations and numbers of crabs and hydrothermal venting features on each face of the edifice were recorded and densities were computed.

2.3. Mussel size estimation

Sizes (shell length) of individual mussels were measured in 3DMetrics. Due to the large number of mussels observed on the edifice, not all visible individuals could be measured. Therefore, measurements were carried out on a subset of randomly selected mussel assemblage polygons. The number of mussels to be measured for size was estimated with a power analysis. Based on an intermediate effect size and a significance level of 0.05, the power analysis indicated that at least 64 mussels per assemblage and per face should be measured to detect potential size differences between assemblages and faces of the edifice. For each mussel assemblage category on a given face, seven polygons were randomly selected and, within each polygon, 10 mussels were haphazardly chosen for size measurement (representing a total of 70 mussels measured per assemblage category and per edifice face). To do so, random numbers were generated in R (R Core Team 2017), and polygons associated with these numbers were analyzed. Only polygons with a surface larger than 0.01 m² (large enough to contain at least 10 mussels) were included in this analysis. Within each polygon, only mussels for which the entire shell length was visible were measured.

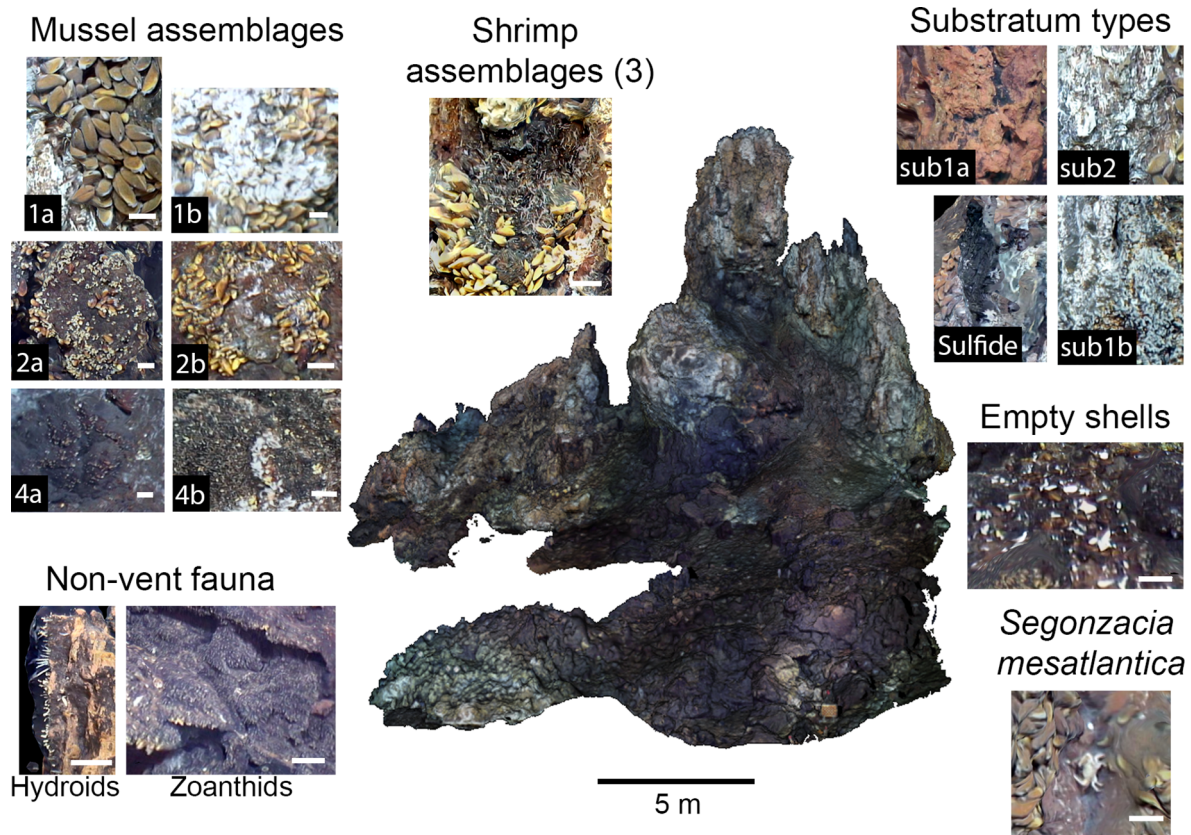


Fig. 2. 3D model of Eiffel Tower facing south with identified and digitized fauna and substrata. Mussel assemblages: (1) Dense beds of large *Bathymodiolus azoricus* mussels with (b) or without (a) microbial filaments; (2) Clumps of medium-sized *B. azoricus* mussels with (b) or without (a) microbial filaments; (4) Sparse and very small *B. azoricus* mussels with (b) or without (a) microbial filaments. Substratum types: (sub1) Bare substratum with (b) or without (a) a microbial cover; (sub2) Bare substratum with anhydrite precipitation. Unless indicated otherwise, all scale bars represent a distance of 5 cm.

The resolution of the 3D model did not always allow for the analysis of seven polygons per assemblage category and per face, or the measurement of 10 mussels per polygon. Overall, a total of 2599 mussels (assemblage 1a: 349, assemblage 1b: 261, assemblage 2a: 554, assemblage 2b: 570, assemblage 4a: 547, assemblage 4b: 318) were measured.

Average mussel size was estimated for all mussel assemblages. As mussels belonging to assemblage 2 (clumps of medium-sized mussels) covered the widest range of sizes, their average size was also calculated for each face of the edifice.

2.4. Temperature measurements

A “chain” made of a series of 100 interconnected digital thermistors was deployed on Eiffel Tower in 2016 during the annual EMSO-Azores maintenance expedition (Cannat and Sarradin, 2016; Matabos et al. 2018; Appendix A: Fig. A1). These thermistors were in contact with the sulfide substrata and recorded temperatures every 5 min for a period of 3 months (from 16 October 2016 to 18 January 2017). Bottom water temperature was measured by a temperature probe mounted on the current meter deployed in 2016 (see description below).

The type of assemblage or substratum in contact with each thermistor was recorded. Average temperatures and standard deviations associated with each assemblage or substratum were then calculated based on the average temperatures and associated standard deviations measured by each probe over the study period. Due to the low representation of certain assemblages in the dataset, only the main faunal assemblage categories (1, 2, 4, shrimps, zoanthids) were considered. No distinction was made between assemblages covered with microbial filaments and those free of microbial cover.

2.5. Estimation of the distance from hydrothermal features

Due to the large number of polygons associated with each faunal assemblage, a subset of randomly selected polygons was also used in this analysis. In the case of mussel assemblages, polygons initially selected for mussel size measurements were used. Polygons corresponding to shrimp and zoanthid assemblages were randomly selected using the same method as for mussel assemblages (Section 2.3). Seven shrimp polygons per face were selected when possible (shrimp assemblages were not present on every face), resulting in a total of 38 selected polygons. Because zoanthids were only observed on the southern periphery of the edifice, 38 polygons (equivalent to the total number of selected shrimp polygons) instead of 7 were selected.

All distance measurements were computed in the 3D point cloud processing software CloudCompare© (v2.10). Spatial coordinates of all polygons (point at the center of each polygon) and *S. mesatlantica* crabs as well as coordinates of all smokers and flanges were extracted from 3DMetrics and subsequently imported into CloudCompare©. Distances between each polygon or crab and the nearest smoker or flange were then calculated and average distances between crabs or each assemblage category and hydrothermal venting features were estimated.

2.6. Terrain variable measurements

Terrain variables were also computed in CloudCompare©. The high-resolution 3D model was imported into the software and converted to a point cloud. The point cloud was then split in two using the segmentation tool (Appendix A: Fig. A2). This step was necessary to prevent CloudCompare© from comparing two points located on opposite sides of the edifice. Point clouds corresponding to each half of the edifice

were thus analyzed separately (southern half: $n = 1\,000\,169$ points; northern half: $n = 999\,838$ points).

Roughness and slope values were then computed for each point of the clouds. Roughness was analyzed at two different scales: a small scale (10 cm) to measure the microtopography of the edifice and roughness associated with assemblage 1 (underlying substratum not visible), and a large scale (1 m) to quantify the overall topography of the edifice. To estimate roughness, a sphere was centered on each point of the 3D point clouds, and the roughness value of any given point was equal to the distance between this point and the best fitting plane computed based on all the points present within the sphere. Slope values were computed on a scale of 1 m. For that, normal vectors (vectors indicating the orientation of the model surface) associated with each point of the clouds were first computed using a 1 m radius and then oriented using the minimum spanning tree method. They were then converted into dip values (between 0 and 90°) giving the angle between the best fitting plane and the horizontal plane.

Average roughness and slope values were measured for the entire edifice as well as for each face separately. Randomly selected polygons (Section 2.5) were used to estimate the average roughness and slope associated with each faunal assemblage. Additionally, the average roughness and slope within each randomly selected polygon were recorded. For simplification, only the main faunal assemblage categories (1, 2, 4, shrimps, zoanths) were considered.

2.7. Interaction between bottom currents, topography and smoker locations

A modeling approach was employed to quantify the exposure of the different habitats to hydrothermal fluid exiting from main or secondary vents. The effect of bottom currents on plume dispersal and assemblage distribution has never been evaluated at such a small spatial scale (few meters). A relatively simple model, that did not include bottom boundary layer or microturbulence processes generated by topography, was thus chosen as a first step to initiate this investigation. The model used bottom current, smoker location and topography data to first identify smokers exposed to currents based on their location, compute the reach of vent fluids exiting these smokers, and then calculate the cumulative daily exposure to currents potentially bringing plume material at each location (see Data S1 for model code).

Current data included in the model were collected using a TCM3 Lowell Instrument seabottom current meter deployed 20 m south of the southern periphery domain of Eiffel Tower (N37 17.328 W32 16.540, 1697 m depth; Fig. 1) in 2016 (Cannat and Sarradin, 2016; Cannat et al. 2017). The current meter recorded the direction and velocity of currents in the bottom 1.5 m of the water column every minute between September 2016 and July 2017. Spatial coordinates of the entire 3D model point cloud were extracted in CloudCompare© and used to build the bathymetry for the model. Although the datasets included in the model were collected in different years (2016–2017 for currents and 2015 for topography and smoker and assemblage locations), the remarkably high stability of the edifice (Cuvelier et al. 2011b) combined with the absence of significant changes in the distribution of assemblages, microbial mats and smokers between 2015 and 2016 (unpublished results) indicate that these differences in data collection year will not affect our conclusions.

The model involved three steps. First, smokers not shielded from current by topographic features (favorable vents) were identified for all current directions (0–360°). Plume heights of 3 m and 1 m were considered to assess the shielding effect of relief on main and secondary smokers, respectively. These values were chosen conservatively based on field observations and temperature measurements suggesting that plumes significantly dilute with seawater at higher heights.

Then, the “visibility” of each habitat from every favorable vent was evaluated based on the distance, azimuth and depth difference between habitats and favorable vents. It was assumed that habitats 1 m (main smokers) or 0.5 m (secondary smokers) deeper than favorable vents

were out of reach for the current-entrained plume material. We also assumed that plume material would be effectively diluted with seawater for habitats located more than 5 m (main smokers) or 1 m (secondary smokers) away from favorable vents. These distances were informed by visual field observations. The 1 m distance limit set for secondary smokers was defined based on results showing that large mussels, which rely on vent fluid for their nutrition, were generally observed between 50 cm and 2 m away from smokers (Cuvelier et al. 2009), this study).

Finally, the exposure of every “visible” habitat to favorable currents (currents potentially carrying plume material from favorable vents) was estimated. Both the mean cumulative daily exposure to favorable currents and the mean velocity of these favorable currents were calculated for each habitat over a period of 312 days. The cumulative daily exposure to favorable current was expressed as a fraction of the day under favorable currents. Note that this number may be greater than 1 because, within a given day, habitats could be exposed to currents coming from several favorable vents. This calculation did not include the possibility for current-entrained hydrothermal plume material to go up-slope on intervening relief as commonly observed in video observations.

Two types of analysis, involving different habitats of interest, were carried out. The aim of the first analysis was to map the exposure to favorable currents (currents potentially carrying plume material) throughout the entire edifice. To do so, a 40 cm bathymetric grid was defined over the entire edifice and grid points were used as habitats in the model. In the second analysis, the exposure to favorable currents was quantified for the different faunal assemblages using the randomly selected polygons (Section 2.5).

As a result, a total of four models were run: two models estimating the exposure to favorable currents for grid points, one based on main smokers and the other on secondary smokers, and two models estimating the exposure to favorable currents for faunal assemblages, also based on main and secondary smokers.

2.8. Statistical analyses

To characterize the distribution of the crab *Segonzacia mesatlantica* and determine whether crabs had a preference for certain types of assemblage or substratum, the null hypothesis that crabs were randomly distributed was tested with a Chi-square test. Expected values were calculated from the proportion of the edifice covered by the different assemblages and substrata. The number of crabs observed on each assemblage or substratum type comprised the observed values that were compared with the expected values.

Correlations between the density of crabs and that of hydrothermal features on each face, and between average medium-sized mussel size and average daily exposure to favorable currents for each face were tested with non-parametric Spearman’s rank correlation tests.

Because the normality and homoscedasticity assumptions necessary to perform ANOVAs were not met, non-parametric Kruskal-Wallis tests were conducted to test for differences in mussel size, distance from hydrothermal features, roughness, slope, temperature and temperature standard deviation between assemblages or faces of the edifice. When significant, Dunn’s post-hoc rank sum comparisons, available in the “dunn.test” (v.1.3.5) R package, were carried out. In the case of roughness and slope, averages obtained for the different faunal assemblages were compared to each other as well as to average values obtained for the entire edifice (used as a reference).

To investigate the relationships between terrain variables and faunal assemblages, multinomial logistic regression models were tested using the “nnet” (v.7.3.12) R package. To allow for comparisons between all assemblage categories, four multinomial models, including the different faunal assemblages (1, 2, 4, shrimp and zoanths) as response categories, were run, each time with a different category used as reference. In all models, distance from smokers, distance from flanges,

small-scale roughness (10 cm), large-scale roughness (1 m), and slope were included as predictors. Additionally, quadratic discriminant analyses (QDA) were conducted using the “MASS” (v.7.3.47) R package to evaluate prediction accuracy for all faunal assemblages (1, 2, 4, shrimp and zoanths) based on the following predictors: distance from smokers, distance from flanges, small-scale roughness (10 cm), large-scale roughness (1 m) and slope. All possible combinations of predictors were tested and the proportion of polygons correctly classified after cross validation was recorded for each combination. Data associated with the randomly selected polygons (Sections 2.5 and 2.6) were used in both the multinomial regression and QDA analyses. Predictor variables were centered prior to analysis due to scale differences between variables. In the case of the QDA, Box-Cox transformations were applied to all predictor variables to satisfy the assumption of multivariate normality.

3. Results

3.1. Fauna and substrata distribution

The 2015 3D model of Eiffel Tower represented a surface of 452 m² divided into seven faces based on their orientation and position on the edifice (Fig. 1). Hydrothermal activity was variable between faces (Figs. 1–3A). The west side of the tower was the least active with only

one flange, followed by the southern periphery, although all three hydrothermal feature types (main smokers, secondary smokers and flanges) were present. The largest densities of hydrothermal venting features were observed on the east side of the tower and on the northern periphery. Unlike the northern periphery, where only smokers with relatively low fluid fluxes (secondary smokers) were observed, multiple main smokers with high flow rates were identified on the east side. Similar densities of hydrothermal venting features were observed on the remaining faces, which could still be distinguished by the presence (south side of the tower and western periphery) or absence (north side of the tower) of main smokers.

Eiffel Tower was dominated by *Bathymodiolus azoricus* assemblages, which covered about 60% of the edifice (Fig. 3B). The distribution of the different assemblages and substrata varied across the seven faces. The west and north sides of both the tower and periphery were almost entirely (between 81 and 87%) colonized by mussels, with medium-sized mussels (assemblages 2a and 2b) constituting the dominant assemblage. Conversely, nearly half of the east and south sides of the tower were characterized by higher proportions of microbial and anhydrite covers than the other faces. Finally, the southern periphery also showed a low proportion of faunal colonization and was dominated by bare substratum. This face was characterized by the presence of a unique

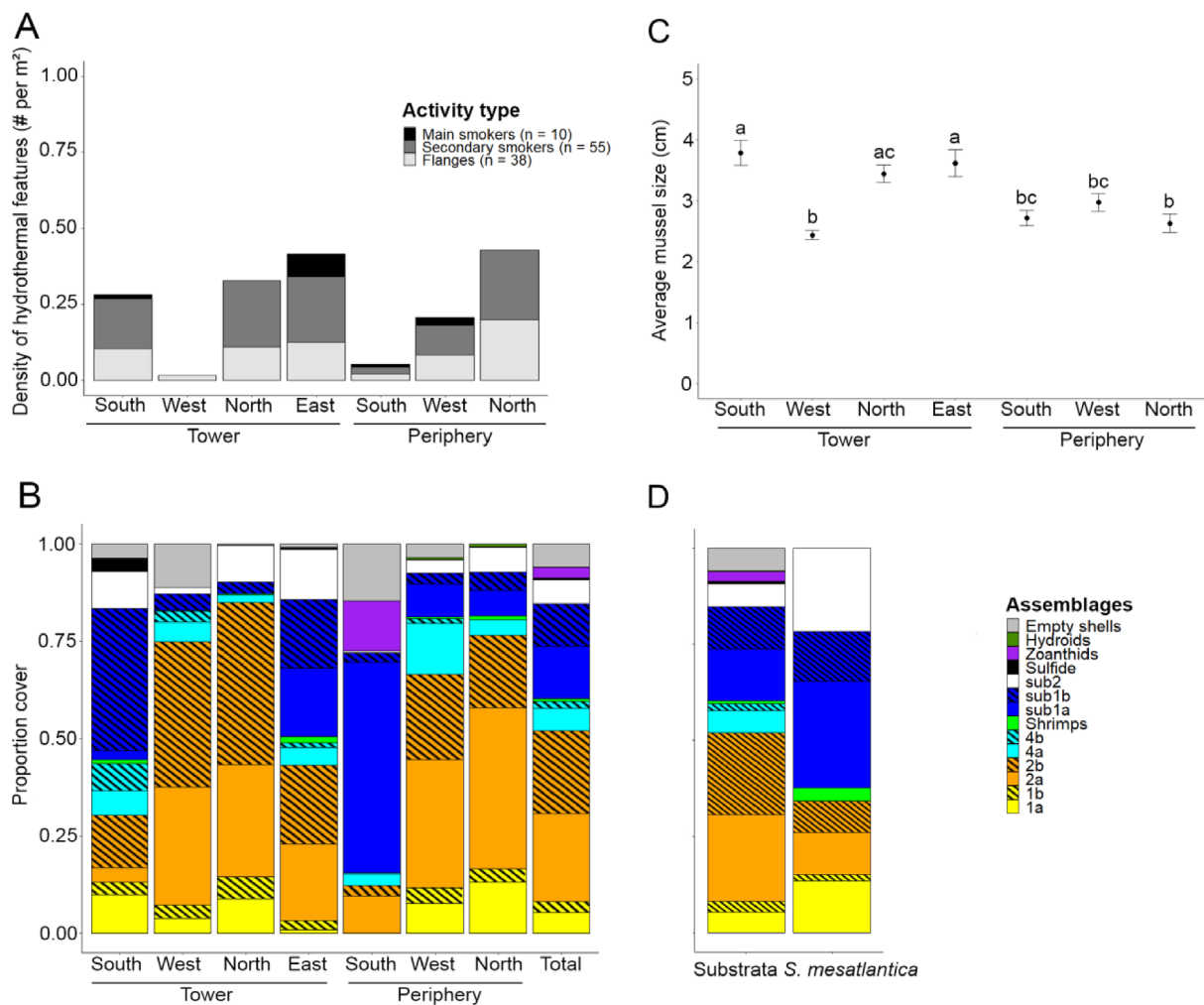


Fig. 3. Fauna, substrata and hydrothermal activity distribution characterized from the 2015 3D model of Eiffel Tower. (A) Density of hydrothermal features on the different faces of the edifice. (B) Proportion cover of all assemblages and substrata on the different faces and on the entire edifice. (C) Average (\pm SE) size of mussels belonging to assemblage 2 on the different faces of the edifice (n = 1125). Size differences were tested with Kruskal-Wallis tests followed by post-hoc Dunn’s rank tests. Different letters indicate faces that were significantly different. (D) Proportion of *Segonzacia mesatlantica* crabs (n = 200) observed on the different assemblages and substrata (observed values) compared with the proportion of the edifice covered by the different assemblages (expected values in the Chi-square test).

assemblage of zoanths (13% cover) and the highest cover of empty *B. azoricus* shells (14%).

A total of 200 *Segonzacia mesatlantica* crabs were observed on the edifice. Crab densities varied among faces and were significantly positively correlated with the density of hydrothermal venting features (Spearman's rho = 0.812, p-value = 0.023). On average, crabs were observed within $2 \text{ m} \pm 2 \text{ m}$ (SD) and $1.4 \text{ m} \pm 1.2 \text{ m}$ (SD) of smokers and flanges, respectively. They were not randomly distributed on the edifice (Chi-square: 155.091, p-value < 0.001), and were observed preferentially on assemblage 1a (large mussels without microbial cover), shrimp assemblages, substrata sub1a and sub1b (bare substratum with or without microbial filaments), and substratum sub2 (anhydrite deposit) (Fig. 3D). Inversely, crabs were associated with assemblages 2a and 2b (medium-sized mussels with or without microbial cover) significantly less often than expected, and were never observed on assemblages 4a or 4b (small mussels with or without microbial cover), or on zoanths.

Mussel sizes were very similar to values obtained for collected mussels measured in laboratory, attesting to the robustness of 3D-based measurement methods (Cuvelier et al. (2011a); Appendix A: Fig. A3). Overall, size differences between assemblages were significant (Kruskal-Wallis test: p-value < 0.001). Post-hoc Dunn's rank comparisons indicated that mussels from assemblage 1 were significantly the largest (average size: $5.96 \text{ cm} \pm 1.44 \text{ cm}$ (SD)), followed by assemblage 2 (average size: $3.27 \text{ cm} \pm 1.49 \text{ cm}$ (SD)) and assemblage 4 (average size: $1.15 \text{ cm} \pm 0.629 \text{ cm}$ (SD)). Except for assemblage 2, where mussels from the 2b assemblage were significantly larger than those from 2a, there were no significant size differences between mussels covered (b) or not (a) with microbial filaments.

The size of medium-sized mussels (assemblages 2a and 2b) significantly differed between faces of the edifice (Kruskal-Wallis test: p-value < 0.001) (Fig. 3C). The largest mussels were observed on the south, north and east sides of the tower, this result being significant for the east and south sides. On the tower, the mussels from assemblage 2 observed on the western side were significantly smaller than those on the other sides.

3.2. Temperature characterization of microhabitats

Data collected by the digital thermistors suggested that different assemblages and substrata were exposed to different temperatures (Appendix A: Fig A4 & Table A1). On average, assemblages 1 ($6.34 \text{ }^\circ\text{C} \pm 0.575 \text{ }^\circ\text{C}$ (SE)) and 2 ($5.93 \text{ }^\circ\text{C} \pm 0.121 \text{ }^\circ\text{C}$ (SE)) as well as substratum sub1b ($5.92 \text{ }^\circ\text{C} \pm 0.126 \text{ }^\circ\text{C}$ (SE)) were exposed to higher and more variable temperatures than zoanths ($5.39 \text{ }^\circ\text{C} \pm 0.0883 \text{ }^\circ\text{C}$ (SE)), assemblage 4 ($5.59 \text{ }^\circ\text{C} \pm 0.0722 \text{ }^\circ\text{C}$ (SE)) and substratum sub1a ($5.37 \text{ }^\circ\text{C} \pm 0.120 \text{ }^\circ\text{C}$ (SE); Kruskal-Wallis tests; Mean: p-value = 0.0057, SD: p-value = 0.0188). However, these differences were only significant between assemblage 2 or substratum sub1b and substratum sub1a, and between substrata sub1b and sub1a for average temperature and the standard deviation of temperature, respectively. The only thermistor in contact with anhydrite deposits ($6.49 \text{ }^\circ\text{C} \pm 0.361 \text{ }^\circ\text{C}$ (SE)) indicated that this substratum type was exposed to temperatures at least as high and variable as assemblages 1 and 2 and substratum sub1b. On average, all temperatures measured by the thermistors were higher than the average background bottom water temperature ($4.71 \text{ }^\circ\text{C} \pm 0.0697 \text{ }^\circ\text{C}$ (SE)).

3.3. Effects of distance from hydrothermal venting features and terrain variables on faunal assemblage distribution

Distances from smokers or flanges differed significantly between assemblage types (Kruskal-Wallis tests: p-value < 0.001 in all tests; Fig. 4). Shrimp assemblages (3) and assemblage 1 were closest to both smokers and flanges, followed by assemblages 2 and 4, and finally zoanthid assemblages which were located furthest from hydrothermal

venting features. The same patterns were observed when a distinction was made between mussel assemblages covered (b) or not (a) with microbial filaments (Fig. 4).

Roughness (measured on 10 cm and 1 m scales) and slope values were successfully estimated for all points of the 3D point cloud (Appendix A: Fig. A2), and, significantly differed between faces of the edifice (Kruskal-Wallis tests: p-value < 0.001 in all tests; Appendix A: Fig. A5). Similarly, faunal assemblages were associated with significantly different roughness and slope values (Kruskal-Wallis, p-value < 0.001 in all tests; Fig. 5). Shrimp assemblages (3) were associated with the largest roughness values (on both scales), followed by assemblage 1. Both assemblages had roughness values significantly larger than the edifice average. On the small (10 cm) scale, zoanths were associated with roughness values similar to the edifice average, whereas assemblages 2 and 4 were associated with roughness values significantly lower than average. On the large scale, roughness values associated with assemblages 2, 4 and zoanths were all significantly lower than the edifice average with assemblage 2 being associated with significantly larger values than assemblage 4 and zoanths.

Slightly different trends were observed for slope (Fig. 5). The steepest slopes were associated with shrimp assemblages (3), followed by assemblages 1, 4, and then 2, all being significantly steeper than the edifice average. Finally, zoanthid assemblages were associated with significantly lower slope values than the edifice average.

Results from multinomial logistic regression models pinpointed which variables play a significant role in discriminating between faunal assemblages (Appendix A: Table A2). Models testing the effects of distance from hydrothermal features and terrain variables indicated that the distance from smokers had a significant positive effect on the probabilities of belonging to assemblages 2 or 4 compared with the shrimp assemblage and assemblage 1, and on the probability of belonging to the zoanthid assemblage compared with all other assemblages. Distance from flanges had a significant negative effect on the probability of belonging to the shrimp assemblage compared with all mussel assemblages, and a significant positive effect on the probability of belonging to the zoanthid assemblage compared with all other assemblages. In terms of terrain variables, slope had a significant positive effect on the probability of belonging to assemblage 4 compared with assemblage 2, and a significant negative effect on the probability of belonging to the zoanthid assemblage compared with all other faunal assemblages. Finally, large-scale roughness had a significant positive effect on the probability of belonging to the shrimp assemblage compared with assemblages 2, 4 and zoanths.

QDA results corroborated those from the multinomial logistic regression models, showing that, depending on the assemblage, different combinations of predictors were involved in the most accurate classifications (Appendix A: Tables A3). Overall, the zoanthid assemblage and assemblage 2 had the highest proportions of correct classifications (87% of correct classifications). For zoanths, discrimination was optimal when only distance from hydrothermal venting features was used as a predictor. However, in the case of assemblage 2, the best proportion of correct classifications was obtained when small-scale roughness was the only predictor used. Interestingly, classifications for assemblage 2 were the most accurate when distance from smokers and flanges was not included as a predictor. The level of correct classifications dropped for the other assemblages. Distance from smokers and flanges rendered the optimal classification for assemblage 1 (58% of correct classifications). In the case of assemblage 4 and the shrimp assemblage (3), the most accurate classifications were obtained when slope or both small-scale roughness and slope, respectively, were included in addition to distance from hydrothermal features (55% and 50% of correct classifications, respectively).

3.4. Effect of favorable currents on microbial mat and faunal distribution

The velocity and direction of currents, recorded by the current

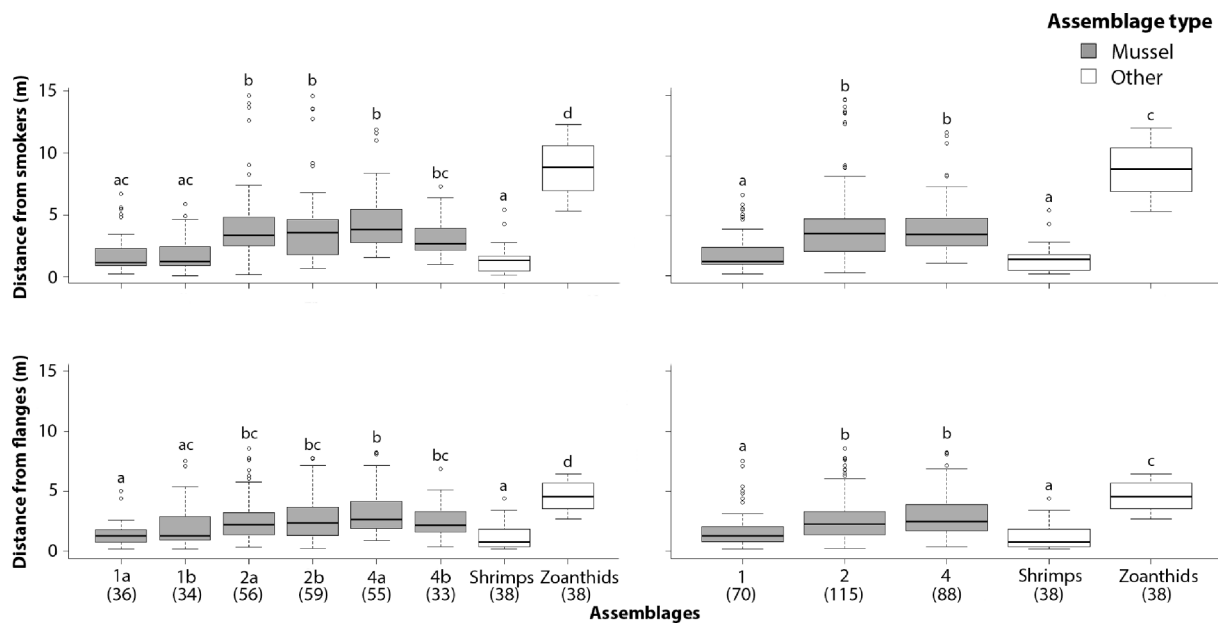


Fig. 4. Distance between the different faunal assemblages and hydrothermal venting features (smokers and flanges) on Eiffel Tower. Differences between assemblages were tested with Kruskal-Wallis tests followed by post-hoc Dunn's rank tests. Different letters indicate assemblages that were significantly different. The number of analyzed polygons associated with each assemblage is indicated in parentheses.

meter deployed south of Eiffel Tower in 2016, were highly variable, even within a single day (Appendix A: Fig A4). Current velocities varied between 2 and 21 cm/s, and current direction changed with tides from dominantly northward to dominantly southward. Lowest current velocities corresponded to periods during which current direction changed.

Overall, bottom-current model simulations resulted in a partial overlap between the mean cumulative daily exposure to favorable currents (currents potentially carrying moderately diluted plume material from surrounding vents) coming from secondary smokers and microbial mat distribution on the edifice (Fig. 6A & B). However, mat distribution could be explained almost entirely once the effect of main smokers was included. Although an average velocity of $9.54 \text{ cm/s} \pm 5.52 \text{ cm/s}$ (SD) (min: 1.79 cm/s; max: 20.7 cm/s) was estimated for favorable currents, the majority of microbial mats under vent influence developed in areas exposed to average current speeds greater than 10 cm/s (Fig. 6A & C).

Exposure to currents, both in terms of exposure time and velocity, varied among assemblages (Table 1). On average, shrimp assemblages had the longest exposure to favorable currents coming from both secondary and main smokers. When considering only secondary smokers, large mussel assemblages were, by far, associated with the highest cumulative daily exposure to favorable currents of all mussel assemblages. Assemblages 2 and 4, in particular, were hardly exposed to any favorable currents from secondary vents. Different patterns were observed for main smokers. Cumulative daily exposure to favorable currents from main vents were similar for all three mussel assemblages with slightly higher values associated with assemblages 2 and 4 than with assemblage 1. Similarly, secondary and main smokers showed different patterns in favorable current velocities. In the case of secondary smokers, the highest velocities were measured for the few small mussel patches exposed to favorable currents. Favorable current velocities associated with assemblages 1 and 2 were similar, whereas they were the lowest for shrimp assemblages. Conversely, favorable currents from main smokers were the fastest over assemblage 1 followed by shrimp assemblages, assemblages 2 and 4. According to the model, zoanthid assemblages were never exposed to favorable currents.

Finally, the average size of medium-sized mussels (2a and 2b assemblages) and the average cumulative daily exposure to favorable currents per face were significantly positively correlated (Spearman's

$\rho = 0.786$, $p\text{-value} = 0.036$).

4. Discussion

We characterized assemblage distribution on Eiffel Tower based on the analysis of a high-resolution 3D model and found that this distribution as well as the degree of colonization by *Bathymodiolus azoricus* mussels varied across the seven studied faces of the active sulfide edifice. Overall, trends in assemblage distribution were very similar to those described in previous studies based on 2D photo mosaics and could be linked to differences in hydrothermal activity between faces (Cuvelier et al., 2009; Cuvelier et al., 2011b). In this study, we quantitatively tested the effect of multiple environmental variables on assemblage distribution and showed that, when considered all together, these variables can explain the distribution of virtually all assemblages.

As in other studies, we found that the distance from hydrothermal venting features (smokers and flanges) best explained faunal distribution (Hessler, 1985; Cuvelier et al., 2009; Podowski et al., 2010; Gerdes et al., 2019). In particular, the crab *Segonzacia mesatlantica* occurred in close proximity to fluid exits with a clear preference for large mussel and shrimp assemblages, as well as for bare substratum with or without a microbial filament cover. Bythograeid crabs are known for their affinity for hydrothermally active areas (Shank et al., 1998; Cuvelier et al., 2009; Podowski et al., 2010) and are well adapted to survive harsh environmental conditions (Mickel and Childress, 1982; Vetter et al., 1987). Although the sulfide tolerance of *S. mesatlantica* has not been characterized, shallow (800 m) Menez Gwen vent field specimens thrive at temperatures between 6 and 21 °C (Hourdez, 2018). Given that most metazoans do not have such tolerances to harsh conditions, hydrothermally active areas likely constitute a predator-free zone for *S. mesatlantica*. Proximity to fluid exits might also explain why crabs were rarely observed on medium-sized and small mussel assemblages, both located in colder habitats. Moreover, isotopic analyses have identified *S. mesatlantica* as both a predator and scavenger, suggesting that crabs could be opportunistically feeding on microbial filaments, smaller organisms associated with mussel assemblages and, occasionally, on the mussels themselves (Colaço et al., 2002; De Buserrolles et al., 2009; Portail et al., 2018). Due to their abundance, which was likely underestimated because those within mussel assemblages were difficult to

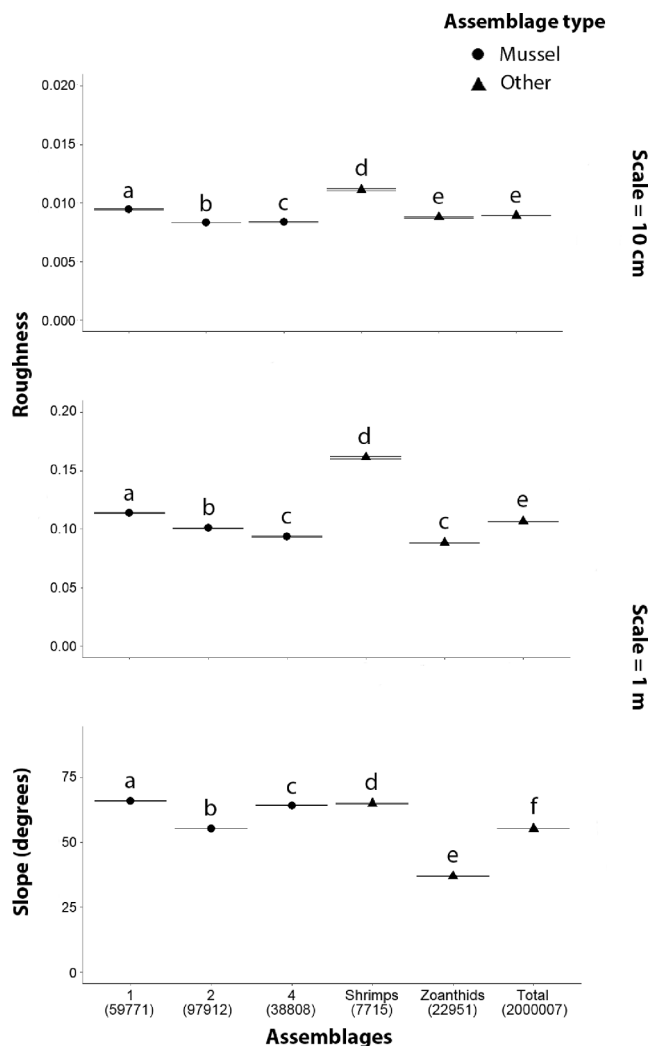


Fig. 5. Average (\pm SE) roughness (on scales of 10 cm and 1 m) and slope (scale of 1 m) measured for the five faunal assemblage types and for the entire edifice (used as a reference for comparisons). Differences between assemblages were tested using Kruskal-Wallis tests followed by post-hoc Dunn's rank tests. Different letters indicate assemblages that were significantly different. The number of points from the 3D point cloud associated with each assemblage is indicated in parentheses.

detect, crabs may play a role in structuring communities on Eiffel Tower, as it is the case for other predators on Pacific vents (Micheli et al. 2002).

Of all faunal assemblages, shrimp assemblages were the closest to fluid exits. *Mirocaris fortunata*, the dominant species in these assemblages is common throughout the Mid-Atlantic Ridge and can withstand temperatures of up to 36 °C (Shillito et al. 2006). This tolerance may explain shrimps' proximity to fluid exits, allowing them to feed on free-living microorganisms entrained by hydrothermal fluid or prey on species associated with nearby mussel assemblages (De Busserolles et al. 2009, Portail et al. 2018).

In contrast, zoanthid assemblages were located the furthest from hydrothermal features. Zoanthids, which have been shown to dominate peripheral communities at other vent sites (e.g. Lau Basin (Sen et al., 2016)) were only observed in the southern periphery, where they covered about a quarter of the area. Like other peripheral taxa, zoanthids are not endemic to vents, but take advantage of their high productivity. Although the trophic ecology of Lucky Strike zoanthids has not been investigated, chemoautotrophic symbioses in cnidarians seem to be unlikely (Childress and Girguis 2011). Instead, zoanthids, which

are suspension feeders, likely prey on small zooplankton feeding on primary productivity or on suspended particles transported via advection (Lonsdale 1977, Enright et al., 1981), justifying their avoidance of stressful conditions associated with venting.

Distance from hydrothermal features also differed between mussel size classes, large mussels being located closest to smokers and flanges, and small mussels the furthest. Segregation by size has been discussed in several studies and linked to *B. azoricus* feeding strategies and temperature tolerance (Comtet and Desbruyères, 1998; Sarradin et al., 1999; Cuvelier et al., 2009; Cuvelier et al., 2011b; Husson et al., 2017). These studies suggest that large mussels rely almost entirely on chemosynthesis and thus need access to sulfide/methane brought by hydrothermal fluids (Fiala-Médioni et al., 2002; Duperron et al., 2006). In contrast, the contribution of suspension feeding seems to increase with decreasing mussel size (Martins et al., 2008; De Busserolles et al., 2009). Moreover, temperatures measured on the different assemblages, which fell within the range of previous studies, imply that large mussels can better cope with high and variable temperatures than small mussels (Cuvelier et al., 2011a; Sarradin et al., 2015; Husson et al., 2017). These studies suggested that mussels probably recruited in cold habitats and then migrated toward warmer habitats as they grew and their energy requirements increased. However, here, the distance from hydrothermal vents did not significantly discriminate medium-sized from small-sized mussel assemblages. The fact that prediction accuracy for the distribution of medium-sized mussels was higher when the distance from hydrothermal features was not included in the analyses further implies that proximity to fluid exits alone is not a good predictor of mussel distribution.

Although the effects of terrain variables (roughness and slope) were less important than the distance from hydrothermal venting features, including them in the analyses did provide additional information on factors driving assemblage distribution. For instance, shrimp assemblages were associated with higher large-scale roughness values than mussels. Shrimps were often observed in concavities, where they probably find shelter from the strong currents measured around the edifice. Although the lower slope values associated with zoanthids are probably a result of their occurrence on the relatively flat base of the edifice, the steeper slopes associated with small mussels may be linked to differential feeding modes. Steep slopes are generally associated with accelerated current velocities. Small mussels are considered to primarily rely on suspension feeding, and a position on a pronounced incline may promote their access to food. While, as previously suggested (Gerdes et al., 2019), terrain variables appear to play only a minor role in structuring vent megafaunal assemblages, it is important to note that the 3D model resolution may not have been sufficiently high to characterize the effect of small-scale roughness and that terrain variables may play a more significant role in structuring macro- and meiofaunal communities (not considered in this study).

Although the effect of hydrothermal plumes at scales of kilometers is relatively well known, this study is the first to document an effect on vent assemblage distribution meters away from fluid exits. Plumes enriched in dissolved chemicals, mineral particulates and microorganisms can rise hundreds of meters from the seafloor and disperse over hundreds of kilometers (Lupton and Craig, 1981; German et al., 2010; Dick et al., 2013). As a result, hydrothermal plumes can globally affect ocean productivity (Cowen et al., 2001; Tagliabue et al., 2010; Levin et al., 2016a). Here, we successfully evaluated the influence of hydrothermal plumes on assemblages at the scale of an entire edifice by modeling the combined effect of bottom currents and topography on plume dispersal.

Our results suggest that differential exposure to relatively undiluted plume material transported by currents influences the distribution of medium-sized and small mussels. As expected, model simulations indicated that, unlike large mussels and shrimps, medium-sized mussel assemblages were rarely exposed to fluid from smokers with moderate to low fluid fluxes (secondary smokers), and small mussel assemblages were almost never exposed due to their distance from fluid exits (the

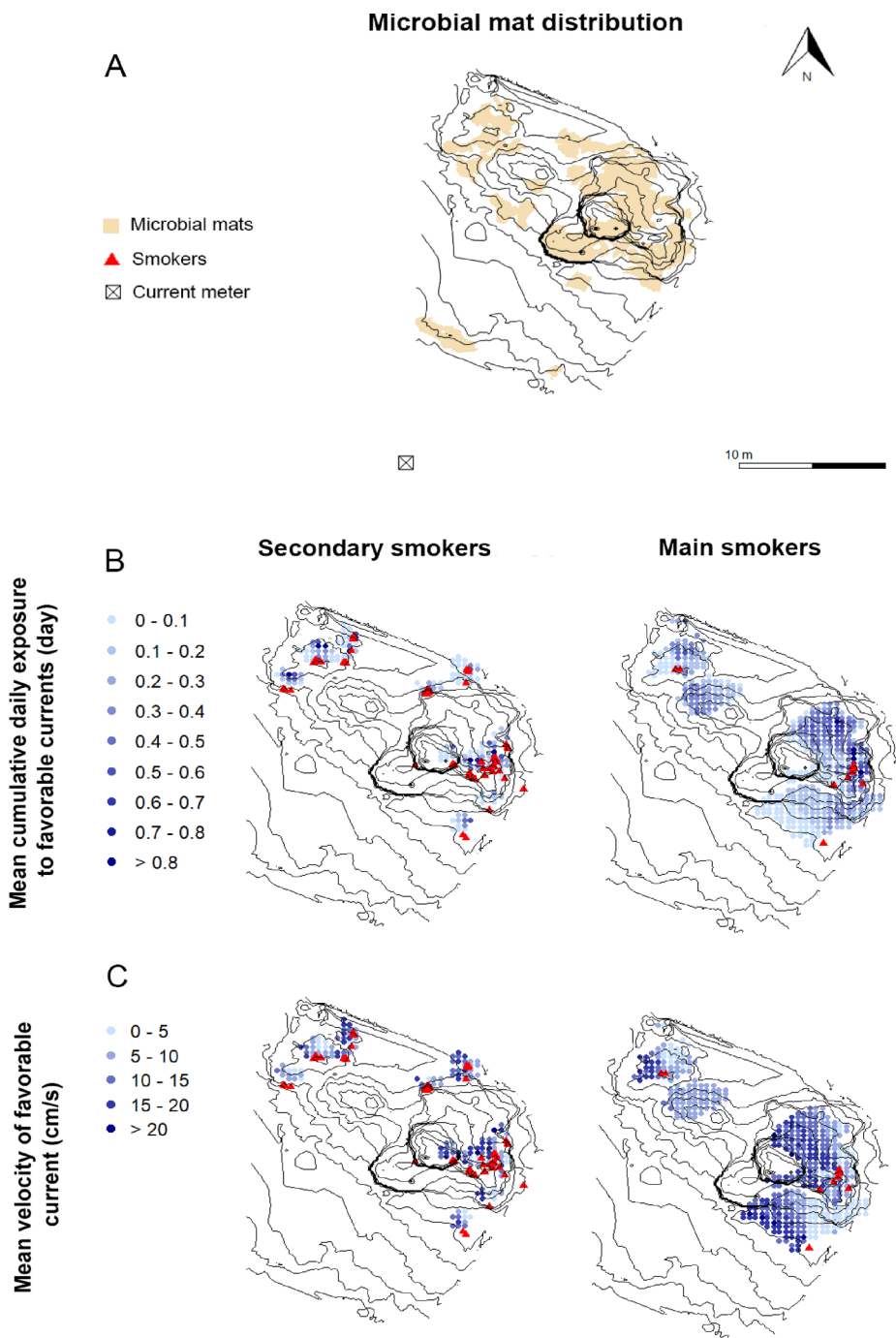


Fig. 6. Relationship between microbial mat distribution and exposure to favorable currents (currents potentially carrying plume material) on Eiffel Tower. Bathymetric maps showing (A) microbial mat distribution over the entire edifice and the location of the current meter, (B) the mean cumulative daily exposure to favorable currents and (C) the mean velocity of favorable currents. Exposure time and favorable current velocity were estimated based on the location of secondary and main smokers separately. Note that the calculated effect of secondary smokers was limited to a distance of 1 m from fluid exits whereas it was limited to a distance of 5 m for main smokers. Also note that calculations did not include the possibility for current-entrained hydrothermal plume material to go upslope on intervening relief as commonly observed in video observations. This limitation likely explains most of the discrepancies between A and B.

influence of secondary smokers was limited to 1 m in the model). However, when main smokers (smokers with larger fluid fluxes) were considered, the model showed that both medium-sized and small mussels were as exposed to plume material as were large mussels. These results indicate that mussel assemblages located in cold microhabitats may still harness energy from vent production. As suggested by chemistry data (Sarradin et al., 1999), although significant dilution occurs as hydrothermal fluid mixes with cold seawater, reduced chemicals as well as plume-associated microorganisms and particles may still reach and fuel assemblages located meters away from smokers. The lower exposure times and favorable current velocities associated with small compared with medium-sized mussels could account for their differential distribution. The observed positive correlation between average exposure time and average mussel size both supports this hypothesis

and explains size differences among faces of the edifice. In particular, the smaller size of mussels on the west side of Eiffel Tower may be due to low exposure to favorable currents resulting in slower growth compared with the rest of the edifice.

Model simulations also indicated that, regardless of current direction, zoanths were never directly exposed to plume material coming from secondary or main smokers. Zoanths appear to be in the edifice’s “blind spot” as the topography prevents currents from pushing vent fluid in their direction. This idea is further supported by the dominance of bare substratum in the southern periphery, where zoanths are found.

The relatively long-distance effect of main smokers on microbial mat distribution was even more striking. Large areas of Eiffel Tower were covered by white filamentous mats which, although dominated by

Table 1

Mean (\pm SE) cumulative daily exposure to favorable currents (currents potentially carrying plume material) and mean (\pm SE) favorable current velocity quantified for all faunal assemblages on Eiffel Tower. Results for both secondary and main smokers are represented. Only assemblages exposed to favorable currents were included in the mean favorable current velocity calculations.

	Assemblage	n	Mean cumulative daily exposure to favorable currents (day)		Mean favorable current velocity (cm/s)			
			Secondary	Main	Secondary	n	Main	n
	1	70	0.0567 (0.0158)	0.0464 (0.0116)	10.4 (1.13)	24	10.5 (1.34)	18
Mussels	2	115	0.0111 (0.0040)	0.0623 (0.0111)	10.6 (1.93)	11	8.98 (1.00)	34
	4	88	0.0013 (0.0008)	0.0510 (0.0114)	15.3 (2.05)	4	8.31 (1.01)	24
Shrimps	38	38	0.154 (0.0357)	0.138 (0.0423)	8.42 (1.13)	23	9.60 (1.28)	14
Zoanthids	38	38	0	0	NA	0	NA	0

sulfur-oxidizing *Beggiatoa* species, comprise diverse microbial communities potentially involved in various metabolic pathways (Crépeau et al., 2011). Microbial mats generally require access to both reduced chemicals and oxygen and thus develop in areas where hydrothermal fluids mix with seawater (Nelson et al., 1989; Teske and Nelson, 2006). Even though in many cases mats developed near flanges, in areas under the influence of secondary smokers or where the presence of anhydrite deposits and shimmering water indicated diffuse venting, their occurrence on large sections of the edifice remained unexplained. For instance, most mats covering the south and east faces of the tower part of the edifice were away from visibly active areas. Here, model results indicated that these zones were actually exposed to currents carrying plume material from main smokers (Fig. 6). White *Beggiatoa* filaments are well adapted to grow in fluctuating environments (Gundersen et al., 1992) and can temporarily persist in the absence of electron donor delivery (McKay et al., 2012). Therefore, concentrations in sulfide, methane or other chemicals present in diluted hydrothermal fluids are likely sufficient for their development. Moreover, the majority of mats were exposed to high current speeds (> 10 cm/s) and the flux of plume-derived material during times spent in favorable currents is likely to increase with current velocity. Although their distribution is often overlooked, microbial mats are crucial members of vent communities. In addition to modifying fluid chemistry (Le Bris et al. 2006), microbial filaments can serve as a food source to many vent organisms (Portail et al. 2018). Studies have shown that the majority of vent-endemic fauna appear to feed on free-living microbes (Govenar 2012). In fact, microbial mats growing meters away from fluid exits, in colder and less toxic habitats, may even serve as a food source for background fauna.

In this study, we used a highly simplified model. The model limited the potential effect of hydrothermal plumes to a distance of 5 m, which is consistent with visual field observations. However, it did not predict the fate of favorable currents following contact with the edifice. Favorable currents are expected to follow the relief and disperse along the edifice's walls, affecting wider areas than predicted in Fig. 6. This diffusion may, at least in part, explain the large estimated proportion of mussel patches not exposed to favorable currents. Moreover, we classified smokers into two categories (secondary or main) based on estimated, not measured, differences in actual fluid flow rates. In the future, using hydrodynamic models that discriminate smokers based on fluid temperature and flow rates, and include bottom boundary layer and turbulence processes generated by the complex topography of the edifice should allow for a more precise assessment of the role of favorable currents in structuring vent communities. To do so, additional

in situ current measurements coupled with hydrodynamics modeling at the edifice scale (centimeters to meter resolution) will be required.

In summary, we successfully characterized faunal distribution on a large hydrothermal edifice based entirely on 3D methods. In addition to being more accurate than 2D image-based analyses, these methods allowed the evaluation of direct (terrain variables) and indirect (interaction with currents) effects of topography on assemblage distribution. For the first time, we quantitatively demonstrated that distance from hydrothermal features and temperature are not always the best indicators of exposure to vent activity, and proposed exposure to favorable currents (currents potentially carrying plume material) as an additional indicator. Our approach has multiple advantages: it is based on non-destructive methods and is thus well adapted for monitoring, and it can be employed to study faunal distribution at large scale on any edifice. Given that bathymodiolin mussels are the most common foundation species in chemosynthetic environments (Govenar 2010), our conclusions likely apply to other vents. Moreover, segregation by size, one of the main foci of this study, has been documented for other taxa (Marsh et al. 2012) and considering the effect of exposure to favorable currents may shed new light on their distribution. Overall, specifying the respective roles of environmental variables, including topography and bottom currents, in shaping communities at vents, but also in other deep environments where currents and topography interact to form highly heterogeneous habitats (e.g. canyons and seamounts) will lead to a better understanding of benthic communities' ability to respond to natural or anthropogenic changes.

Declaration of Competing Interest

The authors declare that they have no known competing financial interests or personal relationships that could have appeared to influence the work reported in this paper.

Acknowledgements

We would like to thank the crews of the RV *Pourquoi pas?* and RV *Atalante* for contributing to the expeditions' success (Momarsat 2015 <https://doi.org/10.17600/15000200> and 2016 <https://doi.org/10.17600/16001200>). We would also like to thank the ROV *Victor6000* team for their valuable help with data collection. We are particularly grateful to all members of the LEP/RDT technical and engineering team involved with the EMSO-Azores observatory for their support on land and at sea. This work was made possible by a grand funded through the ANR Lucky Scales [ANR-14-CE02-0008] as part of the EMSO-Azores research program (<http://www.emso-fr.org/EMSO-Azores>). This manuscript was professionally edited by C. Engel-Gautier.

Appendix A. Supplementary material

Supplementary data to this article can be found online at <https://doi.org/10.1016/j.pcean.2020.102397>.

References

- Aleynik, D., Inall, M., Dale, A., Vink, A., 2017. Impact of remotely generated eddies on plume dispersion at abyssal mining sites in the Pacific. *Sci. Rep.* 7, 16959.
- Arnaubec, A., Opderbecke, J., Allais, A., Brignone, L., 2015. Optical mapping with the ARIANE HROV at IFREMER: The MATISSE processing tool. Pages 1-6 in OCEANS 2015 - Genova.
- Barreyre, T., Escartin, J., Sohn, R.A., Cannat, M., Ballu, V., Crawford, W.C., 2014. Temporal variability and tidal modulation of hydrothermal exit-fluid temperatures at the Lucky Strike deep-sea vent field, Mid-Atlantic Ridge. *J. Geophys. Res. Solid Earth* 119, 2543-2566.
- Buhl-Mortensen, L., Vanreusel, A., Gooday, A.J., Levin, L.A., Priede, I.G., Buhl-Mortensen, P., Gheerardyn, H., King, N.J., Raes, M., 2010. Biological structures as a source of habitat heterogeneity and biodiversity on the deep ocean margins. *Mar. Ecol.* 31, 21-50.
- Cannat, M., Sarradin, P.-M., 2016. MOMARSAT2016 cruise. RV L'Atalante. <https://doi.org/10.17600/16001200>.

- Cannat, M., Wheeler, B., Barreyre, T., Sarradin, P.-M., 2017. Array of Ocean Bottom Tilt Current Meters: data from the EMSO-Azores observatory, 2016-2017. SEANO. <https://doi.org/10.17882/74195>.
- Cannon, G.A., Pashinski, D.J., Lemon, M.R., 1991. Middepth flow near hydrothermal venting sites on the southern Juan de Fuca Ridge. *J. Geophys. Res. Oceans* 96, 12815–12831.
- Childress, J.J., Fisher, C.R., 1992. The biology of hydrothermal vent animals: physiology, biochemistry, and autotrophic symbioses. *Oceanography Marine Biol. Annual Rev.* 30, 337–441.
- Childress, J.J., Girguis, P.R., 2011. The metabolic demands of endosymbiotic chemoautotrophic metabolism on host physiological capacities. *J. Experimental Biol.* 214, 312–325.
- Colaço, A., Dehairs, F., Desbruyères, D., 2002. Nutritional relations of deep-sea hydrothermal fields at the Mid-Atlantic Ridge: a stable isotope approach. *Deep Sea Res. Part I* 49, 395–412.
- Comtet, T., Desbruyères, D., 1998. Population structure and recruitment in mytilid bivalves from the Lucky Strike and Menez Gwen hydrothermal vent fields (37°17'N and 37°50'N on the Mid-Atlantic Ridge). *Mar. Ecol. Prog. Ser.* 163, 165–177.
- Copley, J.T.P., Jorgensen, P.B.K., Sohn, R.A., 2007. Assessment of decadal-scale ecological change at a deep Mid-Atlantic hydrothermal vent and reproductive time-series in the shrimp *Rimicaris exoculata*. *J. Marine Biol. Association United Kingdom* 87, 859–867.
- Cosel, R.V., Comtet, T., Krylova, E.M., 1999. *Bathymodiolus* (Bivalvia: Mytilidae) from hydrothermal vents on the Azores triple junction and the Logatchev hydrothermal field. *The Veliger* 42, 218–248.
- Cowen, J.P., Bertram, M.A., Wakeham, S.G., Thomson, R.E., William Lavelle, J., Baker, E.T., Feely, R.A., 2001. Ascending and descending particle flux from hydrothermal plumes at Endeavour Segment, Juan de Fuca Ridge. *Deep Sea Res. Part I* 48, 1093–1120.
- Crépeau, V., Cambon Bonavita, M.-A., Lesongeur, F., Randrianalivo, H., Sarradin, P.-M., Sarrazin, J., Godfroy, A., 2011. Diversity and function in microbial mats from the Lucky Strike hydrothermal vent field. *FEMS Microbiol. Ecol.* 76, 524–540.
- Cuvellier, D., de Busserolles, F., Lavaud, R., Floch, E., Fabri, M.-C., Sarradin, P.-M., Sarrazin, J., 2012. Biological data extraction from imagery – How far can we go? A case study from the Mid-Atlantic Ridge. *Marine Environ. Res.* 82, 15–27.
- Cuvellier, D., Legendre, P., Laes, A., Sarradin, P.-M., Sarrazin, J., 2014. Rhythms and Community Dynamics of a Hydrothermal Tubeworm Assemblage at Main Endeavour Field – A Multidisciplinary Deep-Sea Observatory Approach. *PLoS ONE* 9, 1–16.
- Cuvellier, D., Sarradin, P.M., Sarrazin, J., Colaço, A., Copley, J.T., Desbruyères, D., Glover, A.G., Santos, R.S., Tyler, P.A., 2011a. Hydrothermal faunal assemblages and habitat characterisation at the Eiffel Tower edifice (Lucky Strike, Mid-Atlantic Ridge). *Mar. Ecol.* 32, 243–255.
- Cuvellier, D., Sarrazin, J., Colaço, A., Copley, J., Desbruyères, D., Glover, A.G., Tyler, P., Serrão Santos, R., 2009. Distribution and spatial variation of hydrothermal faunal assemblages at Lucky Strike (Mid-Atlantic Ridge) revealed by high-resolution video image analysis. *Deep Sea Res. Part I* 56, 2026–2040.
- Cuvellier, D., Sarrazin, J., Colaço, A., Copley, J.T., Glover, A.G., Tyler, P.A., Santos, R.S., Desbruyères, D., 2011b. Community dynamics over 14 years at the Eiffel Tower hydrothermal edifice on the Mid-Atlantic Ridge. *Limnol. Oceanogr.* 56, 1624–1640.
- Davies, A.J., Duineveld, Gerard C.A., Lavaleye, Marc S.S., Bergman, Magda J.N., van Haren, H., Roberts, J.M., 2009. Downwelling and deep-water bottom currents as food supply mechanisms to the cold-water coral *Lophelia pertusa* (Scleractinia) at the Mingulay Reef Complex. *Limnol. Oceanogr.* 54, 620–629.
- De Busserolles, F., Sarrazin, J., Gauthier, O., Gélias, Y., Fabri, M.C., Sarradin, P.M., Desbruyères, D., 2009. Are spatial variations in the diets of hydrothermal fauna linked to local environmental conditions? *Deep Sea Res. Part II* 56, 1649–1664.
- Denny, M.W., 1988. *Biology and the Mechanics of the Wave-Swept Environment*. Princeton University Press, Princeton, New Jersey.
- Desbruyères, D., Biscoito, M., Caprais, J.C., Colaço, A., Comtet, T., Crassous, P., Fouquet, Y., Khripounoff, A., Le Bris, N., Olu, K., Riso, R., Sarradin, P.M., Segonzac, M., Vangriesheim, A., 2001. Variations in deep-sea hydrothermal vent communities on the Mid-Atlantic Ridge near the Azores plateau. *Deep Sea Res. Part I* 48, 1325–1346.
- Dick, G., Anantharaman, K., Baker, B., Li, M., Reed, D., Sheik, C., 2013. The microbiology of deep-sea hydrothermal vent plumes: ecological and biogeographic linkages to seafloor and water column habitats. *Front. Microbiol.* 4.
- Duperron, S., Bergin, C., Zielinski, F., Blazejak, A., Pernthaler, A., McKiness, Z.P., DeChaine, E., Cavanaugh, C.M., Babilier, N., 2006. A dual symbiosis shared by two mussel species, *Bathymodiolus azoricus* and *Bathymodiolus puteoserpentis* (Bivalvia: Mytilidae), from hydrothermal vents along the northern Mid-Atlantic Ridge. *Environ. Microbiol.* 8, 1441–1447.
- Eckman, J.E., 1987. The role of hydrodynamics in recruitment, growth, and survival of *Argopecten irradians* (L.) and *Anomia simplex* (D'Orbigny) within eelgrass meadows. *J. Exp. Mar. Biol. Ecol.* 106, 165–191.
- Enright, J.T., Newman, W.A., Hessler, R.R., McGowan, J.A., 1981. Deep-ocean hydrothermal vent communities. *Nature* 289, 219–221.
- Eriksson, B.K., Rubach, A., Hillebrand, H., 2006. Biotic habitat complexity controls species diversity and nutrient effects on net biomass production. *Ecology* 87, 246–254.
- Fiala-Médioni, A., McKiness, Z., Dando, P., Boulegue, J., Mariotti, A., Alayse-Danet, A., Robinson, J., Cavanaugh, C., 2002. Ultrastructural, biochemical, and immunological characterization of two populations of the mytilid mussel *Bathymodiolus azoricus* from the Mid-Atlantic Ridge: evidence for a dual symbiosis. *Mar. Biol.* 141, 1035–1043.
- Fisher, C.R., Takai, K., Le Bris, N., 2007. Hydrothermal Vent Ecosystems. *Oceanography* 20, 14–23.
- Fouquet, Y., H. Ondreas, J. L. Charlou, J. P. Donval, J. Radford-Knoery, I. Costa, N. Lourenço, T. M. K. and M. K. Tivey. 1995. Atlantic lava lakes and hot vents. *Nature* 377:201.
- Frandsen, R., Dolmer, P., 2002. Effects of substrate type on growth and mortality of blue mussels (*Mytilus edulis*) exposed to the predator *Carcinus maenas*. *Mar. Biol.* 141, 253–262.
- Freestone, A.L., Osman, R.W., 2011. Latitudinal variation in local interactions and regional enrichment shape patterns of marine community diversity. *Ecology* 92, 208–217.
- Gerdes, K., Martínez Arbizu, P., Schwarz-Schampera, U., Schwentner, M., Kihara, T.C., 2019. Detailed Mapping of Hydrothermal Vent Fauna: A 3D Reconstruction Approach Based on Video Imagery. *Frontiers in Marine Science* 6.
- German, C.R., Bowen, A., Coleman, M.L., Honig, D.L., Huber, J.A., Jakuba, M.V., Kinsey, J.C., Kurz, M.D., Leroy, S., McDermott, J.M., de Lépinay, B.M., Nakamura, K., Seewald, J.S., Smith, J.L., Sylva, S.P., Van Dover, C.L., Whitcomb, L.L., Yoerger, D.R., 2010. Diverse styles of submarine venting on the ultraslow spreading Mid-Cayman Rise. *Proc. Natl. Acad. Sci.* 107, 14020–14025.
- Goffredi, S.K., Johnson, S., Tunnicliffe, V., Caress, D., Clague, D., Escobar, E., Lundsten, L., Paudyal, J.B., Rouse, G., Salcedo, D.L., Soto, L.A., Spelz-Madero, R., Zierenberg, R., Vrijenhoek, R., 2017. Hydrothermal vent fields discovered in the southern Gulf of California clarify role of habitat in augmenting regional diversity. *Proc. Royal Soc. B Biol. Sci.* 284, 20170817.
- Govenar, B., 2010. Shaping Vent and Seep Communities: Habitat Provision and Modification by Foundation Species. In: Kiel, S. (Ed.), *The Vent and Seep Biota: Aspects from Microbes to Ecosystems*. Springer, Netherlands, Dordrecht, pp. 403–432.
- Govenar, B., 2012. Energy Transfer Through Food Webs at Hydrothermal Vents Linking the Lithosphere to the Biosphere. *Oceanography* 25, 246–255.
- Grassle, J.F., 1985. Hydrothermal Vent Animals: Distribution and Biology. *Science* 229, 713–717.
- Gundersen, J.K., Jorgensen, B.B., Larsen, E., Jannasch, H.W., 1992. Mats of giant sulphur bacteria on deep-sea sediments due to fluctuating hydrothermal flow. *Nature* 360, 454–456.
- Heck, K.L., Wetstone, G.S., 1977. Habitat Complexity and Invertebrate Species Richness and Abundance in Tropical Seagrass Meadows. *J. Biogeogr.* 4, 135–142.
- Hessler, R.R., 1985. Spatial and temporal variation of giant clams, tubeworms and mussels at deep-sea hydrothermal vents. *Bullet. Biolog. Soc. Washington* 6, 411–428.
- Hourdez, S., 2018. Cardiac response of the hydrothermal vent crab *Segonzacia mesatlantica* to variable temperature and oxygen levels. *Deep Sea Res. Part I* 137, 57–65.
- Husson, B., Sarradin, P.-M., Zeppilli, D., Sarrazin, J., 2017. Picturing thermal niches and biomass of hydrothermal vent species. *Deep Sea Res. Part II* 137, 6–25.
- Johnson, K.S., Childress, J.J., Beehler, C.L., 1988. Short-term temperature variability in the Rose Garden hydrothermal vent field: an unstable deep-sea environment. *Deep Sea Research Part A. Oceanographic Res. Papers* 35, 1711–1721.
- Kelly, N., Metaxas, A., 2008. Diversity of invertebrate colonists on simple and complex substrates at hydrothermal vents on the Juan de Fuca Ridge. *Aquatic Biology* 3, 271–281.
- Köhler, J., Hansen, P.D., Wahl, M., 1999. Colonization Patterns at the Substratum-water Interface: How does Surface Microtopography Influence Recruitment Patterns of Sessile Organisms? *Biofouling* 14, 237–248.
- Koivisto, M.E., Westerbohm, M., 2010. Habitat structure and complexity as determinants of biodiversity in blue mussel beds on sublittoral rocky shores. *Mar. Biol.* 157, 1463–1474.
- Kontar, E.A., Sokov, A.V., 1994. A benthic storm in the northeast tropical Pacific over the fields of manganese nodules. *Deep Sea Res. Part I* 41, 1069–1089.
- Koschinsky, A., Garbe-Schönberg, D., Sander, S., Schmidt, K., Gennerich, H.-H., Strauss, H., 2008. Hydrothermal venting at pressure-temperature conditions above the critical point of seawater, 5°S on the Mid-Atlantic Ridge. *Geology* 36, 615–618.
- Kwasnitschka, T., Hansteen, T.H., Devey, C.W., Kutterolf, S., 2013. Doing fieldwork on the seafloor: Photogrammetric techniques to yield 3D visual models from ROV video. *Comput. Geosci.* 52, 218–226.
- Langmuir, C., Humphris, S., Fornari, D., Van Dover, C., Von Damm, K., Tivey, M.K., Colodner, D., Charlou, J.L., Desonie, D., Wilson, C., Fouquet, Y., Klinkhammer, G., Bougault, H., 1997. Hydrothermal vents near a mantle hot spot: the Lucky Strike vent field at 37°N on the Mid-Atlantic Ridge. *Earth Planet. Sci. Lett.* 148, 89–91.
- Le Bris, N., Govenar, B., Le Gall, C., Fisher, C.R., 2006. Variability of physico-chemical conditions in 9°50'N EPR diffuse flow vent habitats. *Mar. Chem.* 98, 167–182.
- Lee, R.W., Robert, K., Matabos, M., Bates, A.E., Juniper, S.K., 2015. Temporal and spatial variation in temperature experienced by macrofauna at Main Endeavour hydrothermal vent field. *Deep Sea Res. Part I* 106, 154–166.
- Lelièvre, Y., Legendre, P., Matabos, M., Mihály, S., Lee Raymond, W., Sarradin, P.-M., Arango Claudia, P., Sarrazin, J., 2017. Astronomical and atmospheric impacts on deep-sea hydrothermal vent invertebrates. *Proc. Royal Soc B Biol. Sci.* 284, 20162123.
- Levin, L.A., Baco, A.R., Bowden, D.A., Colaco, A., Cordes, E.E., Cunha, M.R., Demopoulos, A.W.J., Gobin, J., Grupe, B.M., Le, J., Metaxas, A., Netburn, A.N., Rouse, G.W., Thurber, A.R., Tunnicliffe, V., Van Dover, C.L., Vanreusel, A., Watling, L., 2016a. Hydrothermal Vents and Methane Seeps: Rethinking the Sphere of Influence. *Front. Mar. Sci.* 3.
- Levin, L.A., Mengerink, K., Gjerde, K.M., Rowden, A.A., Van Dover, C.L., Clark, M.R., Ramirez-Llodra, E., Currie, B., Smith, C.R., Sato, K.N., Gallo, N., Sweetman, A.K., Lily, H., Armstrong, C.W., Brider, J., 2016b. Defining “serious harm” to the marine environment in the context of deep-seabed mining. *Marine Policy* 74, 245–259.
- Little, S.A., Stolzenbach, K.D., Grassle, F.J., 1988. Tidal current effects on temperature in diffuse hydrothermal flow: Guaymas Basin. *Geophys. Res. Lett.* 15, 1491–1494.
- Lonsdale, P., 1977. Clustering of suspension-feeding macrobenthos near abyssal hydrothermal vents at oceanic spreading centers. *Deep Sea Res.* 24, 857–863.
- Lupton, J.E., Craig, H., 1981. A Major Helium-3 Source at 15°S on the East Pacific Rise. *Science* 214, 13–18.

- Luther, G.W., Rozan, T.F., Taillefert, M., Nuzzio, D.B., Di Meo, C., Shank, T.M., Lutz, R.A., Cary, S.C., 2001. Chemical speciation drives hydrothermal vent ecology. *Nature* 410, 813.
- Marsh, L., Copley, J.T., Huvenne, V.A.I., Linse, K., Reid, W.D.K., Rogers, A.D., Sweeting, C.J., Tyler, P.A., 2012. Microdistribution of Faunal Assemblages at Deep-Sea Hydrothermal Vents in the Southern Ocean. *PLoS ONE* 7, e48348.
- Martin, J.W., Christiansen, J.C., 1995. A new species of the shrimp genus *Chorocaris* Martin & Hessler, 1990 (Crustacea: Decapoda: Bresiliidae) from hydrothermal vent fields along the Mid-Atlantic Ridge. *Proc. Biol. Soc. Wash.* 108, 220–227.
- Martins, I., Colaço, A., Dando, P.R., Martins, I., Desbruyères, D., Sarradin, P.-M., Marques, J.C., Serrão-Santos, R., 2008. Size-dependent variations on the nutritional pathway of *Bathymodiulus azoricus* demonstrated by a C-flux model. *Ecol. Model.* 217, 59–71.
- Matabos M., J.-P. Brulport, J. Legrand, B. Moreau, J. Sarrazin, P.-M. Sarradin, M. Cannat. 2018. Thermistor chain temperature data from the EMSO-Azores observatory, 2016–2017. <https://doi.org/10.17882/55541>.
- McClain, C.R., Barry, J.P., 2010. Habitat heterogeneity, disturbance, and productivity work in concert to regulate biodiversity in deep submarine canyons. *Ecology* 91, 964–976.
- McKay, L.J., MacGregor, B.J., Biddle, J.F., Albert, D.B., Mendlovitz, H.P., Hoer, D.R., Lipp, J.S., Lloyd, K.G., Teske, A.P., 2012. Spatial heterogeneity and underlying geochemistry of phylogenetically diverse orange and white *Beggiatoa* mats in Guaymas Basin hydrothermal sediments. *Deep Sea Res. Part I* 67, 21–31.
- Menge, B.A., Lubchenko, J., Ashkenas, L.R., 1985. Diversity, heterogeneity and consumer pressure in a tropical rocky intertidal community. *Oecologia* 65, 394–405.
- Micheli, F., Peterson, C.H., Mullineaux, L.S., Fisher, C.R., Mills, S.W., Sancho, G., Johnson, G.A., Lenihan, H.S., 2002. Predation Structures Communities at Deep-Sea Hydrothermal Vents. *Ecol. Monogr.* 72, 365–382.
- Mickel, T.J., Childress, J.J., 1982. Effects of Temperature, Pressure, and Oxygen Concentration on the Oxygen Consumption Rate of the Hydrothermal Vent Crab *Bythograea thermydron* (Brachyura). *Physiological Zoology* 55, 199–207.
- Morozov, G., Veralde, M.G., 2008. Inertial oscillations as deep ocean response to hurricanes. *J. Oceanogr.* 64, 495–509.
- Moulon, P., P. Monasse, R. Marlet, and Others. 2013. OpenMVG. An Open Multiple View Geometry library. <https://github.com/openMVG/openMVG/>.
- Mullineaux, L.S., Butman, C.A., 1990. Recruitment of encrusting benthic invertebrates in boundary-layer flows: A deep-water experiment on Cross Seamount. *Limnol. Oceanogr.* 35, 409–423.
- Nelson, D.C., Wirsén, C.O., Jannasch, H.W., 1989. Characterization of Large, Autotrophic *Beggiatoa* spp. Abundant at Hydrothermal Vents of the Guaymas Basin. *Appl. Environ. Microbiol.* 55, 2909–2917.
- Petratits, P.S., 1990. Direct and indirect effects of predation, herbivory and surface rugosity on mussel recruitment. *Oecologia* 83, 405–413.
- Pizarro, O., Eustice, R., Singh, H., 2009. Large area 3-d reconstructions from underwater optical surveys. *IEEE J. Ocean Eng.* 34, 150–169.
- Podowski, E.L., Ma, S., Luther, G.W., Wardrop, D., Fisher, C.R., 2010. Biotic and abiotic factors affecting distributions of megafauna in diffuse flow on andesite and basalt along the Eastern Lau Spreading Center, Tonga. *Mar. Ecol. Prog. Ser.* 418, 25–45.
- Polzin, K.L., Speer, K.G., Toole, J.M., Schmitt, R.W., 1996. Intense mixing of Antarctic bottom water in the equatorial Atlantic ocean. *Nature* 380, 54–57.
- Portail, M., Brandily, C., Cathalot, C., Colaço, A., Gélinas, Y., Husson, B., Sarradin, P.-M., Sarrazin, J., 2018. Food-web complexity across hydrothermal vents on the Azores triple junction. *Deep Sea Res. Part I* 131, 101–120.
- R Core Team. 2017. R: A language and environment for statistical computing. R Foundation for Statistical Computing, Vienna, Austria.
- Ravaux, J., Hamel, G., Zbinden, M., Tasiemski, A.A., Boutet, I., Léger, N., Tanguy, A., Jollivet, D., Shillito, B., 2013. Thermal Limit for Metazoan Life in Question. In *Vivo Heat Tolerance of the Pompeii Worm*. *PLoS ONE* 8, e64074.
- Sarradin, P.-M., Cannat, M., 2015. MOMARSAT2015 cruise. RV Pourquoi pas ?. <https://doi.org/10.17600/15000200>.
- Sarradin, P.-M., Caprais, J.-C., Riso, R., Kérouel, R., Aminot, A., 1999. Chemical environment of the hydrothermal mussel communities in the Lucky Strike and Menez Gwen vent fields, Mid Atlantic Ridge. *Cah. Biol. Mar.* 40, 93–104.
- Sarrazin, J., Juniper, K.S., Massoth, G., Legendre, P., 1999. Physical and chemical factors influencing species distributions on hydrothermal sulfide edifices of the Juan de Fuca Ridge, northeast Pacific. *Mar. Ecol. Prog. Ser.* 190, 89–112.
- Sarrazin, J., Legendre, P., de Busserolles, F., Fabri, M.-C., Guilini, K., Ivanenko, V.N., Morineaux, M., Vanreusel, A., Sarradin, P.-M., 2015. Biodiversity patterns, environmental drivers and indicator species on a high-temperature hydrothermal edifice, Mid-Atlantic Ridge. *Deep Sea Res. Part II* 121, 177–192.
- Sarrazin, J., Robigou, V., Juniper, S.K., Delaney, J.R., 1997. Biological and geological dynamics over four years on a high-temperature sulfide structure at the Juan de Fuca Ridge hydrothermal observatory. *Mar. Ecol. Prog. Ser.* 153, 5–24.
- Sen, A., Becker, E.L., Podowski, E.L., Wickes, L.N., Ma, S., Mullaugh, K.M., Hourdez, S., Luther, G.W., Fisher, C.R., 2013. Distribution of mega fauna on sulfide edifices on the Eastern Lau Spreading Center and Valu Fa Ridge. *Deep Sea Res. Part I* 72, 48–60.
- Sen, A., Kim, S., Miller, A.J., Hovey, K.J., Hourdez, S., Luther, G.W., Fisher, C.R., 2016. Peripheral communities of the Eastern Lau Spreading Center and Valu Fa Ridge: community composition, temporal change and comparison to near-vent communities. *Mar. Ecol.* 37, 599–617.
- Shank, T.M., Fornari, D.J., Von Damm, K.L., Lilley, M.D., Haymon, R.M., Lutz, R.A., 1998. Temporal and spatial patterns of biological community development at nascent deep-sea hydrothermal vents (9°50'N, East Pacific Rise). *Deep Sea Res. Part II* 45, 465–515.
- Shillito, B., Le Bris, N., Hourdez, S., Ravaux, J., Cottin, D., Caprais, J.-C., Jollivet, D., Gaill, F., 2006. Temperature resistance studies on the deep-sea vent shrimp *Mirocaris fortunata*. *J. Experim. Biol.* 209, 945–955.
- Spies, F.N., Macdonald, K.C., Atwater, T., Ballard, R., Carranza, A., Cordoba, D., Cox, C., Garcia, V.M.D., Francheteau, J., Guerrero, J., Hawkins, J., Haymon, R., Hessler, R., Juteau, T., Kastner, M., Larson, R., Luyendyk, B., Macdougall, J.D., Miller, S., Normark, W., Orcutt, J., Rangin, C., 1980. East Pacific Rise: Hot Springs and Geophysical Experiments. *Science* 207, 1421–1433.
- St Laurent, L.C., Thurnherr, A.M., 2007. Intense mixing of lower thermocline water on the crest of the Mid-Atlantic Ridge. *Nature* 448, 680–683.
- Tagliabue, A., Bopp, L., Dutay, J.-C., Bowie, A.R., Chever, F., Jean-Baptiste, P., Bucciarelli, E., Lannuzel, D., Remenyi, T., Sarthou, G., Aumont, O., Gehlen, M., Jeandel, C., 2010. Hydrothermal contribution to the oceanic dissolved iron inventory. *Nat. Geosci.* 3, 252.
- Teske, A., Nelson, D.C., 2006. The Genera *Beggiatoa* and *Thioploca*. In: Dworkin, M., Falkow, S., Rosenberg, E., Schleifer, K.-H., Stackebrandt, E. (Eds.), *The Prokaryotes: Volume 6: Proteobacteria: Gamma Subclass*. Springer, New York, New York, NY, pp. 784–810.
- Tippenhauer, S., Dengler, M., Fischer, T., Kanzow, T., 2015. Turbulence and finestructure in a deep ocean channel with sill overall on the mid-Atlantic ridge. *Deep Sea Res. Part I* 99, 10–22.
- Tivey, M.K., Bradley, A.M., Joyce, T.M., Kadko, D., 2002. Insights into tide-related variability at seafloor hydrothermal vents from time-series temperature measurements. *Earth Planet. Sci. Lett.* 202, 693–707.
- Tokeshi, M., 2011. Spatial structures of hydrothermal vents and vent-associated megafauna in the back-arc basin system of the Okinawa Trough, western Pacific. *J. Oceanogr.* 67, 651.
- Toole, J.M., Schmitt, R.W., Polzin, K.L., 1994. Estimates of diapycnal mixing in the abyssal ocean. *Science* 264, 1120–1123.
- Tunnicliffe, V., 1991. The biology of hydrothermal vents: Ecology and evolution. *Oceanography Marine Biol.* 29, 319–407.
- Van Dover, C.L., 2014. Impacts of anthropogenic disturbances at deep-sea hydrothermal vent ecosystems: A review. *Marine Environ. Res.* 102, 59–72.
- Van Dover, C.L., Ardron, J.A., Escobar, E., Gianni, M., Gjerde, K.M., Jaeckel, A., Jones, D.O.B., Levin, L.A., Niner, H.J., Pendleton, L., Smith, C.R., Thiele, T., Turner, P.J., Watling, L., Weaver, P.P.E., 2017. Biodiversity loss from deep-sea mining. *Nat. Geosci.* 10, 464–465.
- Van Dover, C.L., Humphris, S.E., Fornari, D., Cavanaugh, C.M., Collier, R., Goffredi, S.K., Hashimoto, J., Lilley, M.D., Reysenbach, A.L., Shank, T.M., Von Damm, K.L., Banta, A., Gallant, R.M., Götze, D., Green, D., Hall, J., Harmer, T.L., Hurtado, L.A., Johnson, M., McKiness, Z.P., Meredith, C., Olson, E., Pan, L.L., Turnipseed, M., Won, Y., Young, C.R., Vrijenhoek, R.C., 2001. Biogeography and Ecological Setting of Indian Ocean Hydrothermal Vents. *Science* 294, 818–823.
- Vetter, R.D., Wells, M.E., Kurtsman, A.L., Somero, G.N., 1987. Sulfide Detoxification by the Hydrothermal Vent Crab *Bythograea thermydron* and Other Decapod Crustaceans. *Physiol. Zool.* 60, 121–137.
- Vic, C.J., Guila, G.R., Pradillon, F., 2018. Dispersion of deep-sea hydrothermal vent effluents and larvae by submesoscale and tidal currents. *Deep Sea Res. Part I* 133, 1–18.
- Walton, S.F.G., 1946. Effect of water currents upon the attachment and growth of barnacles. *Biolog. Bull.* 90, 51–70.
- Westoby, M.J., Brasington, J., Glasser, N.F., Hambrey, M.J., Reynolds, J.M., 2012. 'Structure-from-Motion' photogrammetry: A low-cost, effective tool for geoscience applications. *Geomorphology* 179, 300–314.
- White, M., I. Bashmachnikov, J. Aristégui, and A. Martins. 2008. Physical Processes and Seamount Productivity. In T. J. Pitcher, T. Morato, P. J. Hart, M. R. Clark, N. Haggan, and R. S. Santos, editors. *Seamounts: Ecology, Fisheries & Conservation*.
- Williams, A.B., 1988. New marine decapod crustaceans from waters influenced by hydrothermal discharge, brine, and hydrocarbon seepage. *Fisheries Bulletin*. 86, 263–287.
- Zhang, Y., Liu, Z., Zhao, Y., Wang, W., Li, J., Xu, J., 2014. Mesoscale eddies transport deep-sea sediments. *Sci. Rep.* 4, 5937.
- Zhou, Y., Zhang, D., Zhang, R., Liu, Z., Tao, C., Lu, B., Sun, D., Xu, P., Lin, R., Wang, J., Wang, C., 2018. Characterization of vent fauna at three hydrothermal vent fields on the Southwest Indian Ridge: Implications for biogeography and interannual dynamics on ultraslow-spreading ridges. *Deep Sea Res. Part I* 137, 1–12.